Elastic electron scattering by fullerene, C_{60}

C. Winstead and V. McKoy
A. A. Noyes Laboratory of Chemical Physics, California Institute of Technology, Pasadena, California, 91125, USA
(Received 12 July 2005; published 17 January 2006)

We report cross sections for elastic scattering of low-energy electrons by fullerene, C_{60}, calculated within the static-exchange approximation. The calculations are carried out via the Schwinger multichannel (SMC) method, equivalent in this case to the standard Schwinger variational principle. Combining the high parallel efficiency of the SMC method with a quadrature specially adapted to the high symmetry of C_{60} facilitates the most demanding step of the calculation and so permits the use of a large basis set. We analyze the structure of the cross section with reference to a simple spherical-shell model, and we compare our results to prior measurements and calculations.

DOI: 10.1103/PhysRevA.73.012711 PACS number(s): 34.80.Bm

I. INTRODUCTION

Fullerene, C_{60}, has attracted a tremendous amount of attention since its discovery [1], and many of its properties are by now well characterized. Interactions between low-energy electrons and gas-phase C_{60}, however, have received comparatively limited study. Most of that attention has been directed to identification of inelastic thresholds (electron-energy-loss spectroscopy) [2–5] or to studies of C_{60}'s highly anomalous electron attachment [5–14], which exhibits a large cross section for *nondissociative* attachment over a wide energy range [5,6,9,11]. Studies of the simplest collision process, elastic scattering, are surprisingly limited. Some information is available from experiment and Born-approximation theory at high impact energies [15,16], but to our knowledge, the only experimental study of low-energy elastic electron-C_{60} collisions remains the 1994 paper of Tanaka and co-workers [17], who reported differential cross sections on a relative scale over limited ranges of energy and scattering angle. Theoretical studies of electron interactions with C_{60} have mostly employed simplified models. Yabana and Bertsch [18] computed electronic-excitation cross sections in the distorted-wave Born approximation using a spherical jellium model of the target; spherical jellium potentials have also been extensively applied to photoabsorption and ionization of C_{60} [19–22,28,29]. Still simpler but nonetheless useful models have been applied for photoionization by Xu and co-workers [23], who employed two types of radial square-well potential, and by Amusia and co-workers [24], who treated the target as a spherical δ-function shell, with the strength of the δ function tuned to produce an $\ell=0$ bound state at 2.65 eV, the observed electron affinity of C_{60} [25] (a more recent determination is 2.69 eV [26]). Amusia and co-workers used the same model to compute the integral electron scattering cross section. More elaborate photoionization calculations, employing the local-density approximation but avoiding the spherical jellium model, have also been carried out [27–29]. Intermediate- and high-energy elastic electron scattering has been studied in the Born approximation [15,16,30]. The only high-level computational study of the low-energy elastic cross section, however, is that of Gianturco and Lucchese [31–33], whose procedure incorporated a full treatment of the direct and exchange interactions and an approximate accounting for polarization. Gianturco and Lucchese also applied a similar procedure to obtain photoionization cross sections [34]. Owing to the size of the target molecule, they employed a very restricted basis set (3-21G, in the usual notation) to describe the target wave function.

Our aim in the present study is to obtain a well-converged static-exchange cross section that may be directly comparable to experiment at higher energies, where the neglected polarization effects are less important, and that may also serve as a point of reference for more elaborate calculations. To that end, we apply the Schwinger multichannel (SMC) method [35] in its parallel implementation [36,37]. The most time-consuming step in the calculation is greatly accelerated by adopting a quadrature that fully exploits the high symmetry of C_{60}. The resulting cross sections reveal a rich resonant structure. We analyze that structure with the aid of a simple, semiempirical spherical model and by reference to the unoccupied molecular orbitals of C_{60}. As we will see, both points of view are important to understanding the low-energy resonance structure in our cross section.

II. COMPUTATIONAL DETAILS

The SMC method and its implementation have been discussed in detail elsewhere [35–37]. Here we give only details specific to the present calculations.

All calculations were carried out in the fixed-nuclei approximation. I_h symmetry was assumed, and the C-C bond distances were those determined by Hedberg *et al.* [38].

The ground state of the molecule was computed in the restricted Hartree-Fock (RHF) approximation using the electronic structure program GAMESS [39] and its internal basis sets. Exploratory calculations were carried out with the 3-21G basis set, which is the same basis set as used in the studies of Gianturco and co-workers [31–34]. Final results were obtained using the 6-31G(*d*) basis set, together with the following supplemental set of Gaussians at the center of the C_{60} cage: five *s* functions, with exponents 3.0, 1.0, 0.35, 0.12, and 0.04; four *p* functions, with exponents 1.0, 0.35, 0.12, and 0.04; and three *d* functions, with exponents 0.5, 0.2, and 0.1. No eigenvalues of the Gaussian overlap matrix

fell below the GAMESS warning threshold of 10^{-5}, so numerical linear dependence should not be a problem in this basis set. The "3*s*" $(x^2+y^2+z^2)$ linear combination of each Cartesian *d* orbital was excluded, leaving a total of 872 molecular orbitals (180 occupied and 692 virtual) to be formed from the 935 contracted Gaussians. The variational basis for the scattering problem consisted of the 692 doublet configuration state functions formed from the RHF ground state and each of the virtual orbitals.

The most demanding computational task in our implementation of the SMC method is the evaluation of the interaction-free Green's function for the target and incident electron. By introducing a spectral representation, this task can be reduced to numerical quadrature over a wave vector $\vec{k}$. The three-dimensional quadrature over $\vec{k}$ is carried out as a product of quadratures in the magnitude $|\vec{k}|$ and in the polar angles (θ_k, ϕ_k) that orient the unit vector $\hat{k}$. The angular integrations are of the form

$$\int\int \sin(\theta_k) d\theta_k d\phi_k \langle \chi_m | V | \Phi_0 \exp(i\vec{k}\cdot\vec{r}_{N+1}) \rangle \times \langle \Phi_0 \exp(i\vec{k}\cdot\vec{r}_{N+1}) | V | \chi_n \rangle, \quad (1)$$

where $\chi_{m,n}$ are $(N+1)$-particle configuration state functions, V is the electron-molecule interaction potential, and Φ_0 is the N-electron molecular ground-state wave function. The Dirac brackets indicate integration over the electronic coordinates $\vec{r}_1, \vec{r}_2, \ldots, \vec{r}_{N+1}$. The matrix elements $\langle \chi_m | V | \Phi_0 \exp(i\vec{k}\cdot\vec{r}_{N+1}) \rangle$ can be expressed as linear combinations of readily computable one- and two-electron integrals involving Gaussians and a plane wave. A molecule as large as C_{60} poses a challenge because the number of two-electron integrals scales as $N_k N_g^3$, where N_k is the number of (θ_k, ϕ_k) quadrature points and N_g is the number of contracted Gaussian functions used to represent Φ_0 and the χ_m.

For general molecules, the numerical integration over (θ_k, ϕ_k) is best carried out using the quadratures of Lebedev [40], which are two-dimensional quadratures specifically designed for integrals on the sphere. Not only are Lebedev quadratures efficient, but they also possess octahedral symmetry, so that in molecules belonging to any subgroup of O_h, many points can be obtained by symmetry rather than explicitly evaluated. However, the octahedral symmetry of the Lebedev grids is ill-suited to the icosahedral symmetry of C_{60}, and evaluating the Green's function would require numerical integration over one quarter of the sphere. That is quite feasible for small $|k|$ but grows extremely expensive for large $|k|$, where many points are needed to achieve an adequate angular density.

The high symmetry of C_{60} suggests an alternate approach. If C_{60} were spherical, all directions of $\vec{k}$ would be equivalent, and a *single* (θ_k, ϕ_k) angle would suffice for the Green's-function quadrature. Because C_{60} is nearly, but not quite, spherical, we can hope to replace such a single-point quadrature with quadrature over a finite but small solid angle. Specifically, we note that all 60 carbons are equivalent. Thus after projecting the molecular frame onto the unit sphere, we can partition that sphere into 60 equivalent "Voronoi polygons" [41], each defined as the set of points nearest a given carbon atom. It is easy to see that each such polygon is a spherical triangle whose vertices are the centers of the three faces (two hexagons and a pentagon) surrounding the chosen carbon, and that any such polygon can be transformed into any other under operations of the I_h point group. Moreover, these Voronoi triangles are isosceles, with halves that are equivalent under a reflection. Thus our numerical integration need only extend over one half of one such triangle—a solid angle of $4\pi/120 = \pi/30$ steradian. This economy of a factor of 30 compared to integrating over a quarter sphere makes it much easier to achieve a high density of quadrature points.

To complete the angular integration, we could apply the group operations to map the chosen Voronoi cell to the full (θ_k, ϕ_k) sphere. However, it is much simpler to observe that the integrand in Eq. (1) is totally symmetric; therefore the integral vanishes unless χ_m and χ_n belong to the same component of the same irreducible representation. In the nondegenerate A_g and A_u representations, we need only multiply the integral over the cell by the appropriate scale factor, and in each degenerate representation of I_h, we can obtain the integral by averaging together the results for each component of that representation and scaling up to the full sphere.

For this scheme to work, care must be taken on two technical points. First, the χ_m must be fully classified by symmetry, so that, for example, those χ_m transforming as T_{1u} are subdivided into *x*-, *y*-, and *z*-type blocks. We must then impose a consistent sign convention across all components of a given degenerate representation. One way to do that is to perform a trial evaluation of Eq. (1) using Lebedev quadrature, then flip signs in the virtual orbitals as necessary to impose consistent signs. Both of these steps can be automated to reduce the chance of errors.

In implementing the above procedure, we oriented the molecule so that the *z* axis passed through the center of a pentagonal face and the *yz* plane through the carbon at one of that pentagon's vertices, which carbon was chosen as the center of the Voronoi triangle for the numerical angular integrations in the off-shell portion of the Green's function. Thus those integrations were carried out over the half cell having a vertex at $\theta_k = 0$ and extending from 0 to $\pi/5$ in ϕ_k. To carry out the quadrature within that cell, we used a simple direct product of one-dimensional quadratures in θ_k and ϕ_k, gradually increasing the number of ϕ_k and θ_k points as the magnitude $|\vec{k}|$ increased. For convenience in evaluating the differential cross sections, the on-shell matrix elements were evaluated on Lebedev grids of order 23 below 15 eV, order 35 from 15 to 40 eV, and 41 above 40 eV, sufficient to insure that partial cross sections for different components of a given irreducible representation differ by no more than two parts in 10^5 below 40 eV. The numerically intensive steps were performed on a Xeon cluster using 128 processors in parallel; pre- and post-processing was done in single-processor mode on Xeon work stations.

Eigenphase sums are extremely useful in analyzing the resonance structure. In past work, we have computed eigenphases from the partial-wave representation of the *S* matrix, $S(\ell, m; \ell', m')$. In the present work, we avoid a partial-wave expansion by diagonalizing *S* in the plane-wave representation, $S(\hat{k}, \hat{k}')$; because our scattering amplitude is computed

on a quadrature grid, a finite-matrix representation of $S(\hat{k},\hat{k}')$ suitable for diagonalization is easily generated.

To provide a frame of reference for the *ab initio* results, we also evaluated cross sections for an elementary spherical model of C_{60} consisting of an attractive rectangular-well potential shell centered at $R=6.7173$ bohr, the radius of C_{60}, and having a thickness equal to twice the covalent radius of carbon, 2.9102 bohr. Similar well-like models have been suggested before [19,23,42,43]. Like Amusia and co-workers [24], we tuned the potential strength to produce a state bound by 2.65 eV, but we required the angular momentum of the 2.65-eV state to be $\ell=1$ rather than 0, because electronic-structure calculations indicate the ground anionic state is ${}^2T_{1u}$. This requirement fixes the well depth at 7.0725 eV; the model has no other parameters. Below 40 eV, we solved the model scattering problem for partial waves up to $\ell=15$, which contributes less than 0.1% of the integral cross section at 40 eV; and from 40 to 100 eV, we retained partial waves up $\ell=24$, so errors due to omission of higher waves should be negligible. Rassat and Bensimon [43] used a similar model to study bound states and found that their results were insensitive to the model parameters.

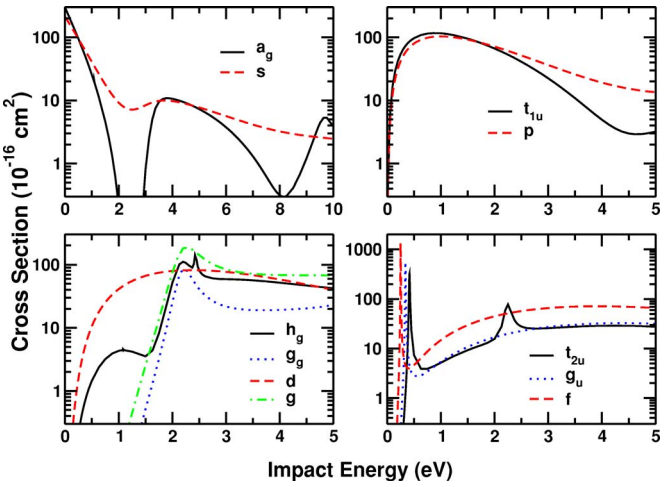

FIG. 1. (Color online) Comparison of low-energy static-exchange integral cross sections with results from the simple spherical-shell model described in the text. *s*, *p*, *d*, *f*, and *g* refer to partial waves from the spherical model; the remaining labels refer to irreducible representations of I_h from the static-exchange calculation.

III. RESULTS AND DISCUSSION

A. Integral cross sections

The lowest four partial waves fall into distinct irreducible representations of the I_h point group: *s* belongs to a_g, *p* to t_{1u}, *d* to h_g, and *f* to t_{2u} and g_u. The first possibility of interference arises with the *g* wave ($\ell=4$), which falls into g_g but also h_g, where it can interact with *d* ($\ell=2$). At low energies, where contributions from higher partial waves are minimized, it is therefore interesting to compare our *ab initio* partial cross sections for the just-named irreducible representations to our spherical-model partial cross sections for the appropriate partial waves. This comparison is shown in Fig. 1. Several remarkable correspondences are evident. In the upper left panel of Fig. 1, we can see that the spherical model produces a minimum at 2.5 eV in the *s*-wave cross section, just where the full static-exchange calculation for a_g shows a (deeper) minimum; there is even a weak undulation in the model result near 8 eV, where the full calculation shows a second minimum. Above the 2.5-eV minimum, the cross section rises fairly quickly to a maximum. Examination of the associated model wave functions and *s*-wave phase shifts reveals a minimum in the phase shift at about 2.4 eV associated with suppression (compared to the potential-free case) of probability density inside the spherical shell, followed by a jump in the phase shift associated with *enhancement* of the probability density inside the spherical shell, indicative of resonant trapping. A nonlinear fit of the model *s*-wave phase shift below 10 eV to the resonant form, using a cubic polynomial in *k* to represent background scattering, gives a position of 3.0 eV and width of 2.2 eV for this "endohedral" resonance; a similar fit to the a_g eigenphase sum below 6 eV gives a position of 3.2 eV and a width of 0.89 eV for its static-exchange counterpart.

As the upper right panel of Fig. 1 shows, both the model *p*-wave result and the full t_{1u} result produce a maximum centered near 1 eV, with rough agreement between the two in both magnitude and width, but with little suggestion of a resonance in either case; below 5 eV, there is only a very weak secondary maximum in the static-exchange cross section near 4.5 eV. In the lower left panel of Fig. 1, we compare the *d* and *g* waves from the model with the static-exchange results for g_g and h_g. The strong resonance at 2.3 eV in the model *g* wave is clearly also present in the g_g and h_g cross sections, less than 0.1 eV lower in energy. At first glance, though, there is seemingly little resemblance on the low-energy side of the resonance between the *d*-wave and h_g cross sections. We may account for the suppression of h_g relative to *d*, however, by invoking destructive interference between the *d* and *g* contributions to h_g. The resonant jump in the *g*-wave phase shift as we move across the resonance profile causes the relative phases of *d* and *g* to change quickly, giving rise to the window-and-peak structure seen in the h_g partial cross section. Looking next at the lower right panel of Fig. 1, we see that the spherical-shell model produces an extremely strong and narrow *f*-wave resonance at 0.250 eV and a broad, nonresonant maximum near 4 eV. Once more, both of these features are echoed in the results from the full calculation for the corresponding representations, t_{2u} and g_u.

Both bound and unbound orbitals of C_{60} are commonly classified as σ or π according to whether they have zero or one radial node located near the carbon cage. As we saw above, the *s*-wave resonance is endohedral and so does not fit well into the σ/π classification. In contrast, the associated radial wave functions indicate that the *f*- and *g*-wave spherical-model resonances are associated with a buildup of probability density within the attractive shell, with no radial node there; thus they (and the related t_{2u}, g_u, g_g, and h_g resonances) can be classified as σ. However, like the *s*-wave resonance, these resonances have no molecular-orbital counterparts.

The absence of sharp low-energy shape resonances associated with the s, p, and d waves is easily understood. As mentioned above, the model potential is chosen to support a p bound state at −2.65 eV, and it naturally supports an s state as well, at −3.43 eV. Examination of the phase shifts shows that not only those for s and p but also that for d go to π, rather than zero, at zero energy (after imposing the asymptotic condition $\delta_\ell \to 0$ as $E \to \infty$); thus the model potential also supports a bound d state, though we did not determine its binding energy. Because true bound states exist for these lowest angular momenta, the first strong quasibound, resonant states are seen at $\ell = 3$ and above.

Considering the results shown in Fig. 1 as a whole, we may observe that the spherical model, despite its extreme simplicity, is surprisingly successful in its qualitative, and even semiquantitative, predictions compared to the far more elaborate static-exchange calculation. Comparison with the model results, moreover, allows us to conclude that some of the most prominent features of the static-exchange cross section—the minimum near 2.5 eV in a_g and the lowest-energy resonances in g_g, h_g, t_{2u}, and g_u symmetries—are "generic" or global properties of a C_{60}-like object that can have little connection to its detailed structure, since they all appear in a nearly structureless model. (The δ-function shell potential of Amusia and co-workers [24] also predicts these features, though somewhat broadened and shifted to higher energies.) Indeed, only in h_g did we see a clear signature of less-than-spherical target symmetry, in the form of interference between the d and g waves.

When the collision energy is more than a few eV, it is no longer possible to associate each irreducible representation of I_h with just one or two partial waves. However, we may extend the utility of our spherical model by resumming its cross sections into I_h components. That is, we treat each partial wave as a reducible representation of the I_h subgroup and perform the reduction to determine weighting factors by which each partial cross section of the spherical model is partitioned among the irreducible representations of I_h [44,45]. Note that this is only a repartitioning of the spherical results; we are not introducing any perturbation to break the spherical symmetry. The results are shown in Fig. 2. Clearly, there is strong qualitative agreement between the spherical-model results and the full static-exchange calculation all the way up to 30-eV collision energy.

Despite the apparent successes of the simple spherical model, there are many features of the full static-exchange cross section that it cannot explain. Some of these are already visible in Fig. 1, where we can see a sharp peak on the high-energy side of the lowest h_g resonance as well as a second peak in t_{2u} at 2.3 eV, neither of which is predicted by the spherical model. Still more unaccounted-for resonances are visible in Fig. 2. However, as we will now discuss, many of these features can be understood in terms of the empty valence molecular orbitals of C_{60}.

In Table I, we collect the energies of the first "extra" resonance in each irreducible representation—that is, the first resonance not accounted for by the spherical-shell model—and we compare those energies to the energies of the lowest unoccupied orbitals from a Hartree-Fock calculation using the MINI [46] minimal basis set, all of which are of π^* type.

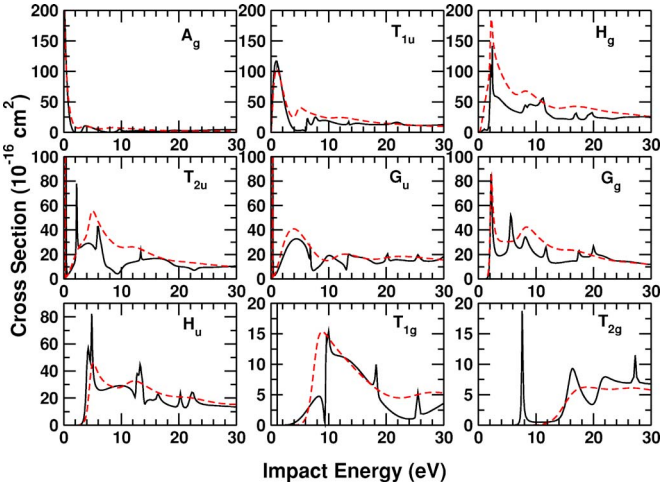

FIG. 2. (Color online) Comparison between the contribution of different irreducible representations of I_h to the static-exchange cross section (solid curves) and the corresponding components as derived by resumming the spherical-shell model cross section (dashed curves); see text for discussion. The a_u contribution, which is extremely small, is not shown.

As may be seen, the correlation is quite good, with the resonance energies being on average about 1.4 eV below the orbital energies. This energy shift is easily accounted for by the difference in basis-set quality between the two calculations, as well as the influence of scattering dynamics. We can therefore say with some confidence that these resonances in our static-exchange cross section are π^* resonances. The fact that they are not seen in our simple model indicates that the more realistic static-exchange interaction is critical to producing them.

At this point it is worth emphasizing that, especially at low collision energies, where the interaction time is long, the static-exchange approximation, which neglects polarization and correlation effects, gives resonance energies that are too high. We thus do not expect the measured resonance energies to coincide with our calculated positions, and indeed, we expect that some of the lowest resonances in the static-exchange cross section will actually correspond to bound excited states of C_{60}^-. In past studies of smaller molecules, we have typically seen energy shifts of 2 to 4 eV for narrow, low-energy resonances. Although the enormous polarizability of C_{60} [47] suggests that larger shifts might be possible in the present case, on the other hand, treating an extended object as a single polarizable center seems likely to overestimate the strength of the polarization interaction. Moreover, there is only ~2.2-eV difference between the Hartree-Fock energy of our t_{1u} lowest unoccupied molecular orbital (LUMO) and the experimental electon affinity [25,26]. Inverse photoemission studies using electron impact on condensed-phase C_{60} [48] reveal two additional features within ~2 eV of the first feature, which correlates with the ground $^2T_{1u}$ state of gas-phase C_{60}^-. Supporting calculations [42,48] indicate that the second feature is t_g and the third $t_g + e_g + t_u + a_g$, and that both are of π character. The same calculations indicate that the first excited feature, seen at ~1.1 eV, should be about 0.5 eV closer to the ground fea-

TABLE I. Energies of the lowest resonances not predicted by the spherical-shell model compared with the energies of the lowest unbound minimal-basis-set Hartree-Fock virtual orbitals.

Symmetry	Shape resonance energy (eV)	Virtual orbital energy (eV)	Energy difference
t_{1g}	1.1	1.6	0.5
h_g	2.2	3.8	1.6
t_{2u}	2.3	3.9	1.6
h_u	4.8	6.3	1.5
g_g	5.7	7.3	1.6
g_u	6.8	8.4	1.6
t_{2g}	7.7	8.9	1.2

ture in the gas phase [48], which would place it at about −2.1 eV, taking −2.65 eV as the $^2T_{1u}$ energy. Comparison to our static-exchange resonance energies in Table I thus suggests that our t_{1g} resonance should be shifted downward by ~3.2 eV to become a $^2T_{1g}$ bound anion state. The third inverse-photoemission feature, about 2.0 eV above the first, in part correlates to h_g and t_{2u} in gas-phase C_{60}, suggesting a shift of ~2.9–3 eV for our h_g and t_{2u} resonances, converting them to weakly bound anion states (which may nonetheless give rise to low-energy resonances when vibration is taken into account). Finally, the condensed-phase calculations indicate that the a_g state contributing to the third inverse-photoemission feature "is localized in the center of the C_{60} molecule and does not correspond to any of the *canonical* σ or π resonances" [48]. We may, however, correlate it with the resonance that we see in both our spherical-model *s*-wave cross section and our static-exchange a_g cross section.

From the evidence in the preceding paragraph, it appears that downward energy shifts roughly in the 2.2–3.2-eV range are needed to align the static-exchange resonances with experiment, quite comparable to the shifts seen in smaller molecules. The first actual π resonance therefore should be an h_u resonance at 1.6–2.6 eV, with the g_g resonance at 2.5–3.5 eV, the g_u at 3.6–4.6 eV, and the t_{2g} at 4.5–5.5 eV. The σ resonances that correlate with resonances in the spherical-well model will likewise be shifted. Both the $\ell=3$ resonances appearing in t_{2u} and g_u and the $\ell=4$ resonances in g_g and h_g are likely to join the *s*-wave resonance discussed in the preceding paragraph in becoming bound states. The first σ feature to appear as an actual resonance would then be that associated with $\ell=5$, which in principle contributes to t_{1u}, t_{2u}, and h_u, but which in our static-exchange results (Fig. 2) is seen clearly only in h_u, where $\ell=5$ is the leading partial wave, at 4.25 eV; assuming the same shift, it should appear in experiment around 2–3 eV.

Huang and co-workers [11] observed peaks in the attachment cross section at 0.2, 1.5, 4.5, and 5.5 eV, as well as a shoulder at ~8.0 eV. They interpreted the lowest three peaks as shape resonances, tentatively assigning the 0.2-eV peak to h_g or t_{2u} and the 1.5-eV peak to h_u or g_g. Our predicted resonance positions from the preceding paragraph generally support these assignments, although they suggest that the g_g resonance may lie too high to contribute to the 1.5-eV peak, and that g_g and a_g, as well as t_{2u} and h_g, may contribute to attachment at near-zero energies. Moreover, we can tentatively associate the 4.5-eV attachment peak with the g_u π resonance and the 5.5-eV peak with the t_{2g} π resonance. However, as Fig. 2 shows, there are additional resonances besides the π resonances that must be considered; in particular, there are resonances in t_{1u} and t_{2u} that may also contribute to the 4.5-eV attachment peak, and yet another t_{1u} resonance that may contribute to the 5.5-eV peak. These are probably the lowest-lying of the many σ^* resonances expected in C_{60}; indeed, as seen in Fig. 2, the cross section up to ~30 eV is densely populated with resonances.

Better insight into the dense resonant structure of the cross section may be gained by examining the eigenphase sums, shown in Fig. 3, in conjunction with the partial cross sections shown in Fig. 2. Weak but narrow resonances, in particular, are more readily visible in the eigenphase plot than in the cross sections. The convention followed in plotting Fig. 3, by which the static-exchange eigenphase sums go to zero at zero energy, is correct except for t_{1u}, where a bound state exists and the zero-energy phase shift should be π. For comparison, Fig. 3 also shows the spherical-shell phase shifts for the first several partial waves. As expected from the good agreement of the cross sections seen in Fig. 1,

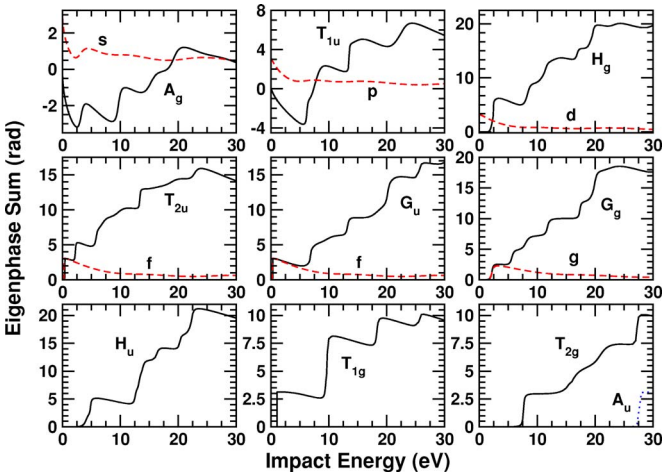

FIG. 3. (Color online) Eigenphase sums in the different irreducible representations of I_h. The curves labeled *s*, *p*, *d*, *f*, and *g* show, for comparison, the leading partial waves in selected representations as computed from the spherical-shell model.

there is good agreement for the first few eV between these phase shifts (modulo π) and the eigenphase sums in the symmetries where they are the leading partial wave; the exception, as noted in the discussion of Fig. 1, is h_g, where not only the leading d wave but also g contributes strongly even at low energies. Some of the notable features at higher energy in Fig. 3 include the clear indication that the t_{1g} feature seen just below 10 eV in Fig. 2 is not one but two overlapping resonances and the presence of a narrow ($\Gamma \sim 0.08$ eV) a_u resonance at about 27.4 eV. Because our a_u variational space is so small, we cannot attach much significance to the computed properties of the latter resonance, but because there is one empty σ valence orbital of a_u symmetry, its existence is not unexpected.

It is interesting, at this point, to compare our results to those of Gianturco and Lucchese [31–33], who carried out prior *ab initio* calculations of low-energy electron-C_{60} scattering. Although the comparison is somewhat complicated by our neglect of polarization and by the sheer number of resonances, some clear points of agreement and disagreement may be seen. In particular, our conclusion above that the lowest π resonance should be an h_u resonance at 1.6–2.6 eV fits well with their results, which show the first resonance to be an extremely narrow h_u resonance at 2.17 eV that is associated with a π-type wave function [33]. On the other hand, both our static-exchange calculation and our spherical-shell model indicate that a σ-type h_u resonance associated with $\ell=5$ should also exist nearby in energy, but Gianturco and Lucchese do not appear to see such a feature. Gianturco and Lucchese predict that the next-lowest resonance should be an a_g resonance at 2.76 eV associated with trapping inside the cage. Although this fits well with both the character and the *unshifted* location of the a_g resonance produced by our static-exchange calculation, as discussed earlier, we expect that inclusion of polarization should shift the latter downward considerably, close to or below 0 eV, where it would correlate with the a_g feature seen in the condensed-phase calculation [48]. Why it should appear so high in energy in the calculation of Gianturco and Lucchese is unclear.

Continuing upward in energy, the next resonance Gianturco and Lucchese see is in g_g, at 3.19 eV, agreeing quite well with the corrected position, 2.5–3.5 eV, that we estimated above for our own π-type g_g resonance. On the other hand, we estimated that the two highest π-type resonances, in g_u and t_{2g}, should occur at 3.6–4.6 eV and 4.5–5.5 eV, respectively, while Gianturco and Lucchese place the g_u resonance at 5.82 eV and the t_{2g} resonance at 6.21 eV, closer than expected to our static-exchange resonance positions. It is possible that the correction we estimated by comparing our lowest-energy resonances to bound states seen in inverse photoemission is too large for these higher-energy resonances. Supporting that interpretation, Gianturco and Lucchese place the first t_{1u} resonance at 5.72 eV, close to our static-exchange energy, 6.2 eV; their first h_g resonance at 7.2 eV, about 1.1 eV below our (third) h_g resonance; and their second t_{1u} resonance at 7.71 eV, almost the same energy as for our second t_{1u} resonance. On the other hand, we see two overlapping t_{1g} resonances at ~9.7 eV where Gianturco and Lucchese see a single resonance at 8.16 eV, and we see a t_{2u} resonance near 5.8 eV while Gianturco and Lucchese predict the first t_{2u} resonance to be at 10.1 eV. On the whole, then, there are some unexplained differences between the two calculations, but for the most part, the low-energy resonances can be cross correlated by allowing for downward shifts of the static-exchange resonance positions by amounts similar to those deduced earlier from comparison with inverse-photoemission and attachment data, perhaps decreasing with increasing collision energy as would be expected.

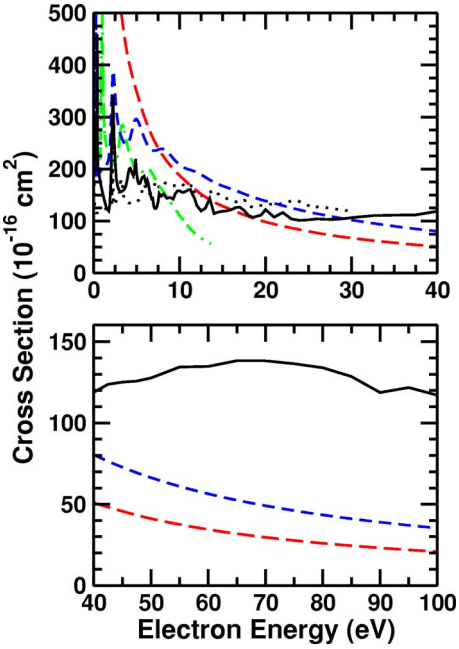

FIG. 4. (Color online) Integral elastic cross section for electron scattering by C_{60}. Solid line: present static-exchange calculation. Dotted line: calculation of Ref. [32]. Long dashes: Born calculation of Ref. [30]. Dot-dashed line: spherical model of Ref. [24]. Short dashes: present spherical model.

In Fig. 4, we compare our static-exchange integral elastic cross section for C_{60} with the predictions of other calculations [24,30,32] and of our own spherical model potential. The simple models produce cross sections that are too large at low energies and too small at high energies, with the cross section from the δ-function shell model of Amusia and coworkers [24] falling off especially quickly. The two high-level calculations—that of Ref. [32] and the present static-exchange result—agree rather well in magnitude and overall trend, despite the differences in resonance positions that were discussed above. An interesting aspect of our static-exchange result is a broad maximum centered at roughly 67 eV that is not predicted by our spherical model. This maximum cannot be attributed to any particular symmetry; rather, it is the net effect of broad maxima that occur between 50 and 90 eV in each symmetry except a_u.

B. Differential cross sections

Low-energy differential cross sections (DCSs) for elastic scattering of electrons by C_{60} are shown at selected energies in Fig. 5. There is good qualitative agreement between the

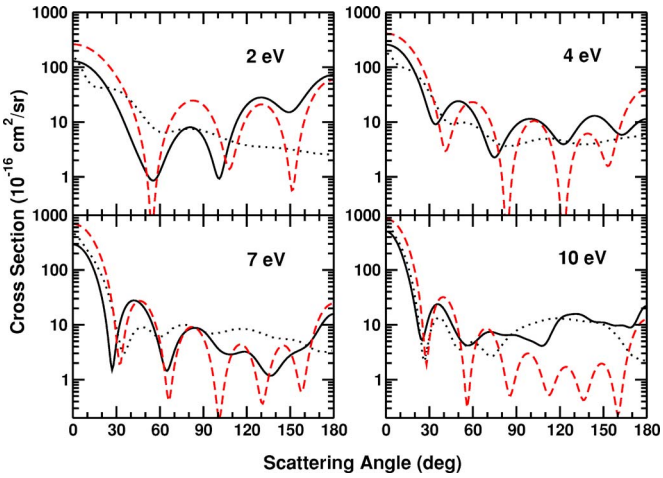

FIG. 5. (Color online) Differential cross sections for electron scattering by C_{60}. Solid line: present static-exchange calculation. Dotted line: calculation of Ref. [32]. Dashed line: present spherical model.

static-exchange and spherical-model results at the lowest energies, with both DCSs exhibiting diffraction-type maxima and minima in approximately the same locations. However, omission of polarization is a major limitation at low energies, and the calculation of Ref. [32], which includes polarization, produces a qualitatively different DCS at 2 and 4 eV. Polarization becomes less important as the energy increases, and indeed, by 10 eV, the two high-level calculations agree fairly well with each other. They also agree qualitatively with the spherical model at near-forward directions, but at higher angles the DCS is enhanced relative to the model and the diffraction pattern is washed out.

At still higher energies, shown in Fig. 6, the same general trend continues: the small-angle DCS exhibits diffraction minima and maxima at the locations predicted by the simple spherical model, while at higher angles the static-exchange DCS is less structured and much larger than the model DCS. At 50 eV, we can also compare the near-forward DCS to the

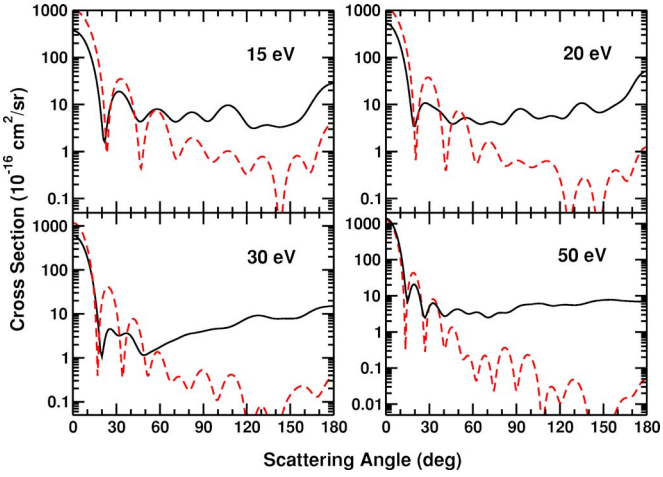

FIG. 6. (Color online) Differential cross sections for electron scattering by C_{60}. Solid line: present static-exchange calculation. Dashed line: present spherical model.

Born-approximation model of Gerchikov and co-workers [30], who computed the DCS up to a momentum transfer of one atomic unit. Their calculation places the first two minima at about 14° and 28°, within 1° of both the static-exchange and spherical-model results. From a semiclassical point of view, we can understand the forward DCS as being dominated by weak collisions at large impact parameters and thus sensitive only to the gross features of the potential that are represented in the model calculations, in particular its radial extent. Conversely, scattering at higher angles involves harder collisions at smaller impact parameters and thus is sensitive to details of the molecular structure. Stronger scattering at high angles appears to be the reason that the static-exchange integral cross section is much larger than the model cross sections at higher energies (Fig. 4). We can verify that the magnitude of the static-exchange DCS at high angles is reasonable by comparing it to that of benzene. At 30 eV and 180°, the C_{60} DCS is 5.67 times larger than our calculated elastic DCS for benzene [49], a reasonable factor; moreover, after scaling up the benzene DCS by that factor at all angles, it differs from the C_{60} DCS by less than 50% over the whole range from 180° down to 85° (though of course the detailed angular dependence of the two DCSs is completely different).

Only limited DCS measurements are available for comparison. Tanaka and co-workers [17] reported measurements of the relative elastic DCSs in which the scattering angle was kept fixed and the energy varied between 1 and 11.5 eV. Their results show broad maxima and minima; for example, the 30° DCS has a single peak, about 4 eV wide, centered near 5 eV, while at 70° there are two peaks, at about 4 and 9 eV, with minima at about 2.5 and 6 eV. Examining our static-exchange DCS at fixed angles as a function of energy reveals essentially no correspondence to the measurements. The calculated DCS has much more structure, owing to the numerous resonances, but only a few broad features, and they do not appear to correlate with those seen in the experiment. Moreover, Tanaka and co-workers [17] estimate the absolute DCS at 7 eV and 30° to be on the order of 400×10^{-16} cm^2; although that value is a very rough estimate, it clearly disagrees with our result (Fig. 5), which is two orders of magnitude smaller. Some of the disagreement in energy dependence is undoubtedly due our omission of polarization and of nuclear vibration, which will affect resonance positions, widths, and intensities in the 1–11.5-eV energy range. Additional measurements, ideally on an absolute scale and over a wider energy and angle range, would be very valuable.

IV. SUMMARY

We have reported cross sections for low-energy elastic collisions of electrons with C_{60} computed in the fixed-nuclei static-exchange approximation. Many features of the static-exchange cross section were shown to be understandable in terms of a simple spherical model; however, the static-exchange results also exhibit features, such as π shape resonances and comparatively strong high-angle scattering, that simple models do not capture. We obtained reasonably good

agreement with the only previous high-level calculation [31–33], considering the limitations of both calculations. Resonance positions appear to correlate fairly well with observed energies of anion states and attachment peaks if allowance is made for a typical downward shift of the static-exchange resonance energies.

ACKNOWLEDGMENTS

This work was supported by the U.S. Department of Energy, Office of Basic Energy Sciences, and employed computational resources of the Caltech-JPL Supercomputing Project.

[1] H. W. Kroto, J. R. Heath, S. C. O'Brien, R. F. Curl, and R. E. Smalley, Nature (London) **318**, 162 (1985).
[2] C. Bulliard, M. Allan, and S. Leach, Chem. Phys. Lett. **209**, 434 (1993).
[3] A. Burose, T. Dresch, and A. Ding, Z. Phys. D: At., Mol. Clusters **26**, S294 (1993).
[4] R. Abouaf, J. Pommier, and S. Cvejanovic, Chem. Phys. Lett. **213**, 503 (1993).
[5] O. Elhamidi, J. Pommier, and R. Abouaf, J. Phys. B **30**, 4633 (1997).
[6] M. Lezius, P. Scheier, and T. D. Märk, Chem. Phys. Lett. **203**, 232 (1993).
[7] D. Smith, P. Španěl, and T. D. Märk, Chem. Phys. Lett. **213**, 202 (1993).
[8] E. Tosatti and N. Manini, Chem. Phys. Lett. **223**, 61 (1994).
[9] T. Jaffke, E. Illenberger, M. Lezius, Š. Matejčik, D. Smith, and T. D. Märk, Chem. Phys. Lett. **226**, 213 (1994).
[10] Š. Matejčik, T. D. Märk, P. Španěl, and D. Smith, J. Chem. Phys. **102**, 2516 (1995).
[11] J. Huang, H. S. Carman, and R. N. Compton, J. Phys. Chem. **99**, 1719 (1995).
[12] C. D. Finch, R. A. Popple, P. Nordlander, and F. B. Dunning, Chem. Phys. Lett. **244**, 345 (1995).
[13] D. Smith and P. Španěl, J. Phys. B **29**, 5199 (1996).
[14] J. M. Weber, M. W. Ruf, and H. Hotop, Z. Phys. D: At., Mol. Clusters **37**, 351 (1996).
[15] L. G. Gerchikov, P. V. Efimov, V. M. Mikoushkin, and A. V. Solov'yov, Phys. Rev. Lett. **81**, 2707 (1998).
[16] Yu. S. Gordeev, V. M. Mikoushkin, and V. V. Shnitov, Mol. Mater. **13**, 1 (2000).
[17] H. Tanaka, L. Boesten, K. Onda, and O. Ohashi, J. Phys. Soc. Jpn. **63**, 485 (1994).
[18] K. Yabana and G. F. Bertsch, J. Chem. Phys. **100**, 5580 (1994).
[19] M. J. Puska and R. M. Nieminen, Phys. Rev. A **47**, 1181 (1993).
[20] G. Wendin and B. Wästberg, Phys. Rev. B **48**, 14764 (1993).
[21] O. Frank and J.-M. Rost, Chem. Phys. Lett. **271**, 367 (1997).
[22] V. K. Ivanov, G. Yu. Kashenock, R. G. Polozkov, and A. V. Solov'yov, J. Phys. B **34**, L669 (2001).
[23] Y. B. Xu, M. Q. Tan, and U. Becker, Phys. Rev. Lett. **76**, 3538 (1996).
[24] M. Ya. Amusia, A. S. Baltenkov, and B. G. Krakov, Phys. Lett. A **243**, 99 (1998).
[25] L.-S. Wang, J. Conceicao, C. Jin, and R. E. Smalley, Chem. Phys. Lett. **182**, 5 (1991).
[26] X.-B. Wang, C.-F. Ding, and L.-S. Wang, J. Chem. Phys. **110**, 8217 (1999).
[27] M. Venuti, M. Stener, G. DeAlti, and P. Decleva, J. Chem. Phys. **111**, 4589 (1999).
[28] P. Decleva, S. Furlan, G. Fronzoni, and M. Stener, Chem. Phys. Lett. **348**, 363 (2001).
[29] A. Rüdel, R. Hentges, U. Becker, H. S. Chakraborty, M. E. Madjet, and J. M. Rost, Phys. Rev. Lett. **89**, 125503 (2002).
[30] L. G. Gerchikov, A. V. Solov'yov, J.-P. Connerade, and W. Greiner, J. Phys. B **30**, 4133 (1997).
[31] R. R. Lucchese, F. A. Gianturco, and N. Sanna, Chem. Phys. Lett. **305**, 413 (1999).
[32] F. A. Gianturco, R. R. Lucchese, and N. Sanna, J. Phys. B **32**, 2181 (1999).
[33] F. A. Gianturco and R. R. Lucchese, J. Chem. Phys. **111**, 6769 (1999).
[34] F. A. Gianturco and R. R. Lucchese, Phys. Rev. A **64**, 032706 (2001).
[35] K. Takatsuka and V. McKoy, Phys. Rev. A **24**, 2473 (1981); **30**, 1734 (1984).
[36] C. Winstead and V. McKoy, Adv. At., Mol., Opt. Phys. **36**, 183 (1996).
[37] C. Winstead and V. McKoy, Comput. Phys. Commun. **128**, 386 (2000).
[38] K. Hedberg, L. Hedberg, D. S. Bethune, C. A. Brown, H. C. Dorn, R. D. Johnson, and M. de Vries, Science **254**, 410 (1991).
[39] M. W. Schmidt, K. K. Baldridge, J. A. Boatz, S. T. Elbert, M. S. Gordon, J. H. Jensen, S. Koseki, N. Matsunaga, K. A. Nguyen, S. J. Su, T. L. Windus, M. Dupuis, and J. A. Montgomery, J. Comput. Chem. **14**, 1347 (1993).
[40] V. I. Lebedev and D. N. Laikov, Dokl. Akad. Nauk **366**, 741 (1999) [Dokl. Phys. **59**, 477 (1999)], and references therein.
[41] E. W. Weisstein, "Voronoi Polygon," http://mathworld.wolfram.com/VoronoiPolygon.html.
[42] J. L. Martins, N. Trouillier, and J. H. Weaver, Chem. Phys. Lett. **180**, 457 (1991).
[43] A. Rassat and D. Bensimon, J. Chim. Phys. Phys.-Chim. Biol. **90**, 1449 (1993).
[44] B. Schmidt and P. Žďánská, Comput. Phys. Commun. **127**, 290 (2000).
[45] H. Bethe, Ann. Phys. **3**, 132 (1929).
[46] S. Huzinaga, J. Andzelm, M. Klobukowski, E. Radzio-Andzelm, Y. Sakai, and H. Tatewaki, *Gaussian Basis Sets for Molecular Calculations* (Elsevier, Amsterdam, 1984).
[47] R. Antoine, Ph. Dugourd, D. Rayane, E. Benichou, M. Broyer, F. Chandezon, and C. Guet, J. Chem. Phys. **110**, 9971 (1999).
[48] M. B. Jost, N. Troullier, D. M. Poirier, J. L. Martins, J. H. Weaver, L. P. F. Chibante, and R. E. Smalley, Phys. Rev. B **44**, 1966 (1991).
[49] M. H. F. Bettega, C. Winstead, and V. McKoy, J. Chem. Phys. **112**, 8806 (2000).